# The Study of Wake Fields in SC Accelerating Cavities

N. Juntong* and R.M. Jones

The University of Manchester and Cockcroft Institute, Manchester M13 9PL, UK.

## Abstract

Each ILC's main linear accelerating cavity, superconducting cavity, is supplied with both fundamental and higher order mode couplers. The configuration of these rf couplers results in an asymmetrical field which gives rise to both an rf kick being applied to the beam and a transverse wake-field. These results can seriously dilute the emittance of the particles beams. Detailed circuit model represent the cavity excluded the couplers are shown in order to assess the loss parameters of cavity. Wake fields of cavity are simulated by using ECHO software benchmarking with ABCI software. The electromagnetic (e.m.) fields are simulated in the vicinity of the couplers in order to assess the impact on the beam dynamics.

## Introduction

The ILC main linacs consist of approximately 16,000 TESLA 9-cell design superconducting rf cavities [1] as shown in Figure 1. A TESLA 9-cell cavity consists of 7 identical mid-cells and 2 tuning end cells. Here we present the initial framework in which we have developed a double chain circuit model for these cavities.

Figure 1: A TESLA 9-cell cavity.

Figure 2: Eigensystem matrix of a double chain circuit model.

$$\eta_{av1}=(\eta_0+\eta_1)/2, \hat{\eta}_{av1}=(\hat{\eta}_0+\hat{\eta}_1)/2$$
$$\eta_{av2}=(\eta_0+\eta_2)/2, \hat{\eta}_{av2}=(\hat{\eta}_0+\hat{\eta}_2)/2$$
$$f_{e1}^2=f_0 f_1, \hat{f}_{e1}^2=\hat{f}_0\hat{f}_1, f_{e2}^2=f_0 f_2, \hat{f}_{e2}^2=\hat{f}_0\hat{f}_2$$

$$w = Eigenvalues[M]$$

$$f = 1/\sqrt{w}$$

$$K_p=\frac{\left|\sum_{n=1}^{N} a_n^{(p)}\sqrt{\varepsilon^{(n)}K_s^{(n)}f_s^{(n)}}\,e^{in\varphi_p}\right|^2}{Nf_p\left(\left|a^{(p)}\right|^2+\left|\hat{a}^{(p)}\right|^2\right)}$$

$$M=\begin{bmatrix}
\frac{1}{f_1^2} & \frac{-\eta_{av1}}{f_{e1}^2} & 0 & \cdots & \cdots & 0 & 0 & \sqrt{\frac{\eta_{av1}\hat{\eta}_{av1}}{4f_{e1}^2\hat{f}_{e1}^2}} & 0 & \cdots & \cdots & 0\\
\frac{-\eta_{av1}}{2f_{e1}^2} & \frac{1}{f_0^2} & \frac{-\eta_0}{2f_0^2} & 0 & \ddots & \vdots & -\sqrt{\frac{\eta_{av1}\hat{\eta}_{av1}}{4f_{e1}^2\hat{f}_{e1}^2}} & 0 & \sqrt{\frac{\eta_0\hat{\eta}_0}{4f_0^2\hat{f}_0^2}} & 0 & \ddots & \vdots\\
0 & \frac{-\eta_0}{2f_0^2} & \ddots & \ddots & 0 & \vdots & 0 & -\sqrt{\frac{\eta_0\hat{\eta}_0}{4f_0^2\hat{f}_0^2}} & \ddots & \ddots & 0 & \vdots\\
\vdots & 0 & \ddots & \ddots & \frac{-\eta_0}{2f_0^2} & 0 & \vdots & 0 & \ddots & \ddots & \sqrt{\frac{\eta_0\hat{\eta}_0}{4f_0^2\hat{f}_0^2}} & 0\\
\vdots & \ddots & 0 & \frac{-\eta_0}{2f_0^2} & \frac{1}{f_0^2} & \frac{-\eta_{av2}}{2f_{e2}^2} & \vdots & \ddots & 0 & -\sqrt{\frac{\eta_0\hat{\eta}_0}{4f_0^2\hat{f}_0^2}} & 0 & \sqrt{\frac{\eta_{av1}\hat{\eta}_{av1}}{4f_{e2}^2\hat{f}_{e2}^2}}\\
0 & \cdots & \cdots & 0 & \frac{-\eta_{av2}}{f_{e2}^2} & \frac{1}{f_2^2} & 0 & \cdots & \cdots & 0 & -\sqrt{\frac{\eta_{av2}\hat{\eta}_{av2}}{4f_{e2}^2\hat{f}_{e2}^2}} & 0\\
0 & 0 & 0 & \cdots & \cdots & 0 & \frac{1}{\hat{f}_1^2} & \frac{\hat{\eta}_{av1}}{2\hat{f}_{e1}^2} & 0 & \cdots & \cdots & 0\\
\sqrt{\frac{\eta_{av1}\hat{\eta}_{av1}}{4f_{e1}^2\hat{f}_{e1}^2}} & 0 & -\sqrt{\frac{\eta_0\hat{\eta}_0}{4f_0^2\hat{f}_0^2}} & 0 & \ddots & \vdots & \frac{\hat{\eta}_{av1}}{2\hat{f}_{e1}^2} & \frac{1}{\hat{f}_0^2} & \frac{\hat{\eta}_0}{2\hat{f}_0^2} & 0 & \ddots & \vdots\\
0 & \sqrt{\frac{\eta_0\hat{\eta}_0}{4f_0^2\hat{f}_0^2}} & \ddots & \ddots & 0 & \vdots & 0 & \frac{\hat{\eta}_0}{2\hat{f}_0^2} & \ddots & \ddots & 0 & \vdots\\
\vdots & 0 & \ddots & \ddots & -\sqrt{\frac{\eta_0\hat{\eta}_0}{4f_0^2\hat{f}_0^2}} & 0 & \vdots & 0 & \ddots & \ddots & \frac{\hat{\eta}_0}{2\hat{f}_0^2} & 0\\
\vdots & \ddots & 0 & \sqrt{\frac{\eta_0\hat{\eta}_0}{4f_0^2\hat{f}_0^2}} & 0 & -\sqrt{\frac{\eta_{av2}\hat{\eta}_{av2}}{4f_{e2}^2\hat{f}_{e2}^2}} & \vdots & \ddots & 0 & \frac{\hat{\eta}_0}{2\hat{f}_0^2} & \frac{1}{\hat{f}_0^2} & \frac{\hat{\eta}_{av2}}{2\hat{f}_{e2}^2}\\
0 & \cdots & \cdots & 0 & 0 & 0 & 0 & \cdots & \cdots & 0 & \frac{\hat{\eta}_{av2}}{2\hat{f}_{e2}^2} & \frac{1}{\hat{f}_2^2}
\end{bmatrix}$$

## A Circuit Model of a Cavity

This model is based upon a double chain circuit model [2] with the N-2 boundary conditions, in which the parameters of the end cells are varied in order to take into account the effects of end cells (which do not have clearly definable coupling parameters or frequencies). Figures 3 to 5 display comparisons of the mode frequency and the kick factors between various circuit models and HFSS [3] simulations. In order to obtain a correct model to represent a TESLA 9-cell structure (without the couplers) we have developed our model by constructing an eigensystem matrix, *M*, in which the mode frequency, *f*, and the mode kick factor, $K_p$, are obtained from the eigenvalues and eigenvectors of the matrix M [2]. We vary the parameters of the end cells to take into account beam tubes and the inherent aperiodic nature of these transitional cells.

The optimized double chain circuit model has an average mode frequency difference of 1.65 and 1.95 MHz and an average kick factor difference of 0.57 and 0.35 V/pC/m/m for the first and the second dipole pass band respectively as shown in Figure 5.

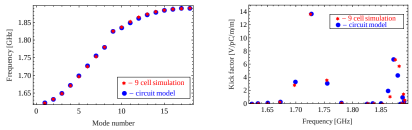

Figure 3: Comparison of the results obtained from the validation of the double chain circuit model with a 9-identical TESLA mid cell shapes structure.

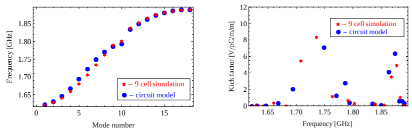

Figure 4: Comparison of the results obtained from the directly applied of a double chain circuit model with a TESLA 9-cell structure without the couplers based on the circuit model of [2].

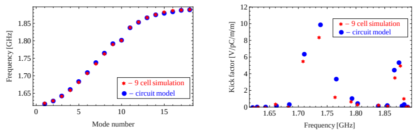

Figure 5: Comparison of the results obtained from the newly developed optimized double chain circuit model for a TESLA 9-cell structure without the couplers.

## Wake Fields of Cavity by ECHO and ABCI

An ultra-relativistic charge particle beams excite wake fields, these wake fields may be decomposed into a short range (within the vicinity of the bunch) and a long range. Here we calculate the proximity or short range wake fields. We simulate wake fields on three different types of accelerating cavities; TESLA, ICHIRO, and RE-ENTRANT as shown in Figure 6. The comparison between ECHO 2D [4] and ABCI [5] results on the longitudinal loss factor ($k_L$) and the transverse loss factor ($k_T$) are shown in Table 1. There are consistent, less than 5% difference, between these two solvers.

| Table 1: Comparison of loss factors between 2 solvers on 3 accelerating cavities. | | $\sigma_z$ = 1 mm | | | $\sigma_z$ = 0.7 mm | | | $\sigma_z$ = 0.3 mm | | |
|---|---|---|---|---|---|---|---|---|---|---|
| | | **ECHO 2D** | **ABCI** | **Δ (%)** | **ECHO 2D** | **ABCI** | **Δ (%)** | **ECHO 2D** | **ABCI** | **Δ (%)** |
| **TESLA** | $k_L$ [V/pC] | 9.89 | 10.04 | 1.52 | 11.56 | 11.82 | 2.25 | 17.72 | 18.46 | 4.18 |
| | $k_T$ [V/pC/m] | 18.36 | 18.52 | 0.87 | 15.41 | 15.61 | 1.30 | 10.38 | 10.57 | 1.83 |
| **ICHIRO** | $k_L$ [V/pC] | 12.89 | 13.03 | 1.09 | 15.32 | 15.57 | 1.63 | 25.19 | 25.77 | 2.30 |
| | $k_T$ [V/pC/m] | 28.14 | 28.26 | 0.43 | 23.94 | 24.06 | 0.50 | 17.03 | 17.12 | 0.53 |
| **RE-ENTRANT** | $k_L$ [V/pC] | 11.01 | 11.15 | 1.27 | 13.08 | 13.34 | 1.99 | 21.25 | 21.91 | 3.11 |
| | $k_T$ [V/pC/m] | 21.17 | 21.30 | 0.61 | 17.96 | 18.14 | 1.00 | 12.70 | 12.85 | 1.18 |

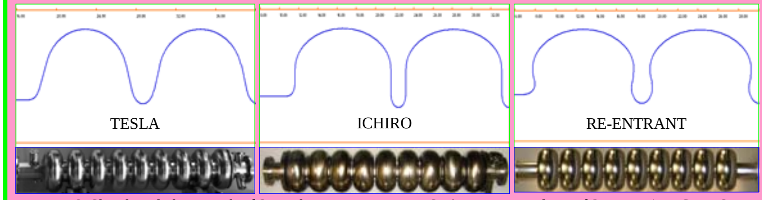

Figure 6: Sketch and photograph of 3 accelerating cavities. TESLA aim at a gradient of 31.5 MV/m, ICHIRO and RE-ENTRANT both are designed to achieve in excess of 50 MV/m.

## Fields in Cavity with Fundamental mode coupler

The inclusion of couplers breaks the cavity symmetry and this affects the transverse fields in the vicinity of couplers. Here we present e.m. fields with the inclusion of the TTF-III type fundamental mode power coupler . The simulation were performed with CST MWS [6] using eigenmode solution. This TTF-III coupler is positioned 45 mm from the end cell and has 9 mm penetration. The simulation were performed with two different boundary conditions at the end of the coupler in order to construct travelling wave solution from two standing wave solution [7] as illustrated in Figure 7. Figure 8 shows the fields along the cavity axis from two boundary conditions at the end of the coupler; electric short (PEC) and magnetic short (PMC). A sufficiently large mesh density is required to resolve the small perturbations for the fields in the vicinity of the coupler.

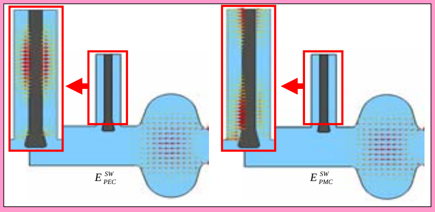

Figure 7: Electric field of 2 standing wave (SW) solutions from 2 boundary conditions at the coupler end. Considering fields inside the coupler region, the traveling wave (TW) solution is obtained from the superposition of 2 SW solutions by the relationship;

$$E^{TW}\propto E_{PMC}^{SW}+iE_{PEC}^{SW}$$

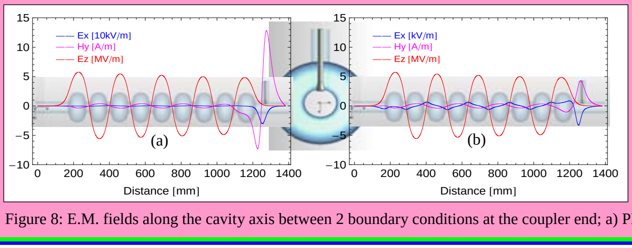

Figure 8: E.M. fields along the cavity axis between 2 boundary conditions at the coupler end; a) PEC, b) PMC.

## RF Coupler Kicks

We construct the travelling wave from two standing wave solutions as the equation below. The coupler kick, *k*, is defined as a ratio of the change in the transverse momentum to the change in the longitudinal momentum [7].

$$E_z=(\xi\hat{E}_{zPM}+i\hat{E}_{zPE})e^{-i(\frac{\omega z}{c}-\phi_k)}$$
$$E_x=(\xi\hat{E}_{xPM}+i\hat{E}_{xPE})e^{-i(\frac{\omega z}{c}-\phi_k)} \quad ; \ \xi=\frac{\left|\hat{E}_{zPE}(x)\right|_{coupler}}{\left|\hat{E}_{zPM}(x)\right|_{coupler}} \ ; \ \Delta p_z c=q\int_{z=0}^{z=L}E_z dz \ ; \ \Delta p_x c=q\int_{z=0}^{z=L}\left(E_x-cB_y\right)dz$$
$$B_y=\mu_0(\hat{H}_{yPE}+i\xi\hat{H}_{yPM})e^{-i(\frac{\omega z}{c}-\phi_k)}$$

The rf coupler kick is given by;

$$k_x=\frac{\Delta p_x c}{\Delta p_z c}=\frac{q\int_{z=0}^{z=L}\left(E_x-cB_y\right)dz}{q\int_{z=0}^{z=L}E_z dz}$$

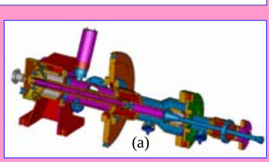

Figure 9: TTF-III power coupler a) cutaway view b) assembly unit.

In the simulations performed on the TTF-III type coupler as shown in Figure 9, the coupler was assumed to be perfectly matched, so the fields are purely incoming in this instance. The rf coupler kick factor is;

$$k_x=(19.74+i91.03)\cdot 10^{-6}$$

## Discussion

The double chain circuit model provides a reasonable model of sc TESLA-like cavities. The kick factors and mode frequencies are well represented after suitable parameterizations. This model lends itself to the inclusion of a study of expected manufacturing errors and their influence on the eigenmodes. This remains a subject of future work. Including rf couplers into the circuit model is also an aspect for future anticipated research.

The CST MWS simulations of the coupler kicks have been obtained by combining two standing wave solutions. More detailed studies will be carried out on the TESLA-style coupler (TTF-III) with the inclusion of the HOM couplers in the near future.

***The issue of the influence of the rf coupler kick on the beam dynamics is considered to be extremely important as if left unsuppressed it is likely to cause severe emittance dilution or possibly a beam break up instability (BBU) in a linear collider or light source.***

## Acknowledgements

We have benefited from discussions at the weekly Manchester electrodynamics and wakefields meeting held at Cockcroft Institute, where these results were first presented. We would like to thank Dr. Igor Zagorodnov for providing permission to use ECHO 2D code.

## References

[1] International Linear Collider Reference Design Report (2007); www.linearcollider.org.
[2] K.L. Bane and R.L. Gluckstern, Part. Accel. 42: p. 123-169, 1993.
[3] www.ansoft.com/products/hf/hfss/
[4] I. Zagorodnov and T. Weiland, Phys. Rev. ST Accel. Beams **8**, 042001 (2005).
[5] Y.H. Chin et al., PAC 2007, THPAN036.
[6] www.cst.com/Content/Products/MWS/
[7] B. Buckley and G.H. Hoffstaetter, Phys. Rev. ST Accel. Beams **10**, 111002 (2007).

**CERN Accelerator School, CAS 2008, Frascati, Italy, 2nd-14th November 2008**

* Nawin.Juntong@postgrad.manchester.ac.uk